Published in final edited form as:
Chemosphere. 2020 May ; 246: 125745. doi:10.1016/j.chemosphere.2019.125745.

Assessing the chemical compositions and disinfection byproduct formation of biofilms: Application of fluorescence excitation-emission spectroscopy coupled with parallel factor analysis

Lei Li[a], **Youchul Jeon**[a], **Hodon Ryu**[b], **Jorge W. Santo Domingo**[b], **Youngwoo Seo**[a,c]

[a]Department of Civil and Environmental Engineering, University of Toledo, Mail Stop 307, 3048, Nitschke Hall, Toledo, OH, USA

[b]Water Systems Division, National Risk Management Research Laboratory, U.S. Environmental Protection Agency, Cincinnati, OH, 45268, USA

Abstract

There are increased concerns over the contributions of biofilms to disinfection byproduct (DBP) formation in engineered water systems (EWS). However, monitoring the biomolecular characteristics of biofilms to understand their impacts on DBP formation has been a great challenge as it requires complex analytical techniques. This study aimed to examine the applicability of fluorescence excitation-emission matrices (EEMs) coupled with parallel factor analysis (PARAFAC) to assess the chemical compositions and DBP formation of biofilms. Biofilms were collected from reactors grown on R2A media, as well as two drinking water-related organic substrates such as humic substances and algal organic matter. The chemical composition and formation of carbonaceous and nitrogenous DBPs of biofilms were continuously monitored every 21 days for 168 days and correlated with the derived EEM-PARAFAC components. Results indicated that all biofilm samples comprised mostly of protein-like components (~90%), and to a lesser extent, humic-like components (~10%). Strong correlations were generally found between tryptophan-like substances and the studied DBP formation ($R^2_{min} \geq 0.76$, $P < 0.05$), indicating that they play a major role in producing biofilm-derived DBPs upon chlorination. Moreover, significant discrepancies between the chemical compositions and DBP formation of biofilms and their corresponding feed solutions were observed, likely due to biotransformation and biosorption processes. Overall, this work highlights that EEM-PARAFAC analysis is a promising tool to monitor the biomolecular characteristics of biofilm components and to predict the subsequent DBP formation in optimizing disinfection protocols for EWS.

[c]Corresponding author. Department of Chemical Engineering, University of Toledo, Mail Stop 307, 3048 Nitschke Hall, Toledo, OH, USA.

CRediT authorship contribution statement

Lei Li: Investigation, Data curation, Methodology, Formal analysis, Writing - original draft, Writing - review & editing. **Youchul Jeon:** Methodology, Formal analysis, Writing - review & editing. **Hodon Ryu:** Formal analysis, Writing - review & editing. **Jorge W. Santo Domingo:** Formal analysis, Writing - review & editing. **Youngwoo Seo:** Conceptualization, Funding acquisition, Project administration, Supervision, Formal analysis, Writing - review & editing.

Declaration of competing interests

We declare that we have no known competing financial interests or personal relationships that could have appeared to influence the work reported in this paper.

Graphical abstract

Graphical abstract

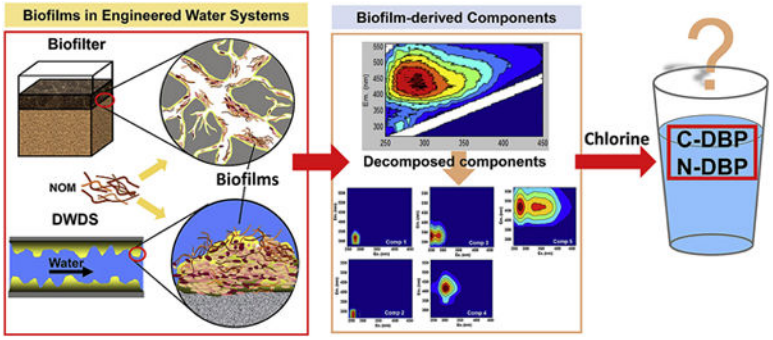

Keywords

Biofilms; Fluorescence excitation-emission matrix; Disinfection byproducts; Correlation; Engineered water systems

1. Introduction

Biofilms are the result of an aggregation of microbial cells embedded in extracellular polymeric substances (EPS), typically comprising of greater than 90% of their total biomass (Liu et al., 2016). Biofilms are widely present in engineered water systems (EWS) (e.g., filtration and drinking water distribution systems), causing critical problems such as filter fouling, opportunistic pathogen growth, biocorrosion, nitrification, and many other issues (Wang et al., 2013a; Liu et al., 2016; Batmanghelich et al., 2017). In order to control biofilm formation in EWS, water utilities apply disinfectants such as chlorine or monochloramines. However, these applied disinfectants can lead to the formation of toxic disinfection byproducts (DBPs) due to the presence of organic-rich substances within biofilms (Zhang et al., 2010; Wang et al., 2013b).

Various operational parameters (e.g., disinfectant concentration, pH, and contact time) are associated with the DBP formation of biofilms (Wang et al., 2012b; Pérez and Susa, 2017). In addition, the intrinsic characteristics of biofilms (e.g., quantity and chemical composition of EPS) significantly affect disinfectant transport and reaction (Xue et al., 2014; Coburn et al., 2016), as well as DBP formation and speciation, where the chemical properties of EPS can be influenced by the organic matter composition in bulk water via their biosorption or biotransformation (Wang et al., 2012a, 2013b; Huang et al., 2013). Different complex organic compounds can be the growth substrate for multispecies biofilms in EWS, including humic substances (HS), a terrestrially-derived allochthonous natural organic matter and algal organic matter (AOM), an algae-derived autochthonous natural organic matter (Camper, 2004; Li et al., 2019). Recently, increased loading of AOM has been a great concern for EWS due to the frequent occurrence of harmful algal blooms in source waters (Pivokonsky et al., 2015, 2016). Although ozone has been widely adopted by water utilities to break down complex organic compounds and reduce DBP formation, ozonation practices can

adversely increase concentrations of assimilable organic carbon (AOC), which in turn can be rapidly utilized and support biofilm growth in downstream filters and distribution systems (Griffini et al., 1999; Polanska et al., 2005). However, our understanding on how these ozonated organic compounds affect the chemical composition and the subsequent DBP formation of biofilms is still very limited, although some studies inferred that biofilm formation could contribute to the increase of DBP formation and distinct DBP speciation in EWS (Baribeau, 2006; Abokifa et al., 2016). Thus, to effectively control biofilms and biofilm-derived DBP formation, probing the chemical properties of biofilms is indispensable.

Conventional methods to analyze the chemical compositions of biofilms include high-performance liquid chromatography and fluorescent microscopy coupled with fluorescent stains for target molecules (Wang et al., 2013b; Xue and Seo, 2013; Matar et al., 2016). However, these methods are time-consuming and costly, and therefore are not suitable for regular monitoring applications at water utilities. Recently, fluorescence excitation-emission matrix (EEM) spectroscopy has received much attention as an efficient and rapid technique to unravel the chemical compositions and molecular structures of organic compounds. Accordingly, several methods have been developed to analyze EEM spectral data, including peak-picking method (Coble, 1996), fluorescence regional integration method (Chen et al., 2003), and more recently, parallel factor (PARAFAC) analysis (Stedmon and Markager, 2005). Among the developed methods, PARAFAC analysis is more sample-specific and can mathematically decompose the complex EEM spectra into several independent fluorescent components consisting of their sources, structures, and chemical reactivities (Henderson et al., 2009; Murphy et al., 2013; Cai et al., 2017). Moreover, the identified EEM-PARAFAC components could be used to predict the DBP formation from different water samples (Lyon et al., 2014; Ma et al., 2018). While this approach holds great potential, to our best knowledge, it has not been applied to evaluate the relationships between the biomolecular composition and DBP formation of biofilms, although biofilm-derived DBP precursors have increasingly been the focus of recent research studies (Pérez and Susa, 2017; Xu et al., 2018; Di Tommaso et al., 2019).

Accordingly, this study aimed to assess the applicability of EEM-PARAFAC analysis for monitoring biomolecular characteristics of biofilm components and their impacts on DBP formation. The chemical composition changes of multi-species biofilms grown on complex organic matter (HS and AOM) were investigated. The correlation between derived EEM-PARAFAC components and DBP formation of biofilms was examined to provide insights into real-time monitoring of DBP formation of biofilms and disinfection optimization for biofilm control in EWS.

2. Materials and methods

2.1. Experimental setup

Fig. S1 shows the schematic diagram of the experiment setup. Mixed-species biofilms (2×10^5 CFU/mL) collected from local water utilities were inoculated into three parallel biofilm reactors (BioSurface Technologies Corp., Boltzmann, MT) with 24 removable coupons installed for each reactor. The reactors were operated at room temperature (24 ± 2 °C) under

dark conditions (Revetta et al., 2016). Biofilms were grown on both sides of the coupons (growth area: 2.50 cm^2) under the same shear stress (100 rpm cylinder rotation speed).

Two biofilm reactors were fed with ozonated HS and AOM. The concentrated HS stock solutions were prepared using a standard chemical (Sigma Aldrich, MO, USA), while the concentrated AOM stock solutions were prepared using cyanobacteria-laden water collected from Lake Erie. The prepared stock solutions were diluted by the granular-activated carbon filtered tap water and treated by coagulation, flocculation, and sedimentation steps. More details for feed solution preparation are available in our previous study (Li et al., 2019). After these conventional treatment processes, the supernatants collected from the sedimentation step were ozonated by 2 mg/L of ozone using a lab-scale ozone generator (OZOTECH, CA, USA) for 5 min. The total organic carbon (TOC) concentration of ozonated solutions was adjusted to 1.5 mg/L, which is a common TOC level found in the EWS in the United States (Baribeau, 2006; Terry and Summers, 2018). Finally, the feed solutions were delivered to HS and AOM biofilm reactors by a multichannel peristaltic pump (Cole-Parmer, IL, USA) with a flow rate of 0.5 mL/min. Additionally, R2A media (Teknova, CA, USA), a commercial nutrient widely used to grow bacteria present in drinking water, was selected as another feed solution for comparison (Reasoner and Geldreich, 1985). To prevent any potential contamination, autoclaved and concentrated R2A stock solutions were directly injected to the R2A biofilm reactor by a syringe pump (KD Scientific, MA, USA) and simultaneously mixed in the reactor with the ozonated tap water (after granular-activated carbon filtration) delivered by a peristaltic pump. The final TOC concentration of influent for the R2A reactor was also maintained at 1.5 mg/L. The reactor influents were replaced every week and stored in a water tank with an air filter to minimize potential microbial growth.

2.2. Water quality of feed solutions and biofilm sampling

Turbidity, pH, TOC, total nitrogen (TN), phosphate (PO_4^{3-}), and specific ultraviolet–visible (UV) absorbance at 254 nm ($SUVA_{254}$) of feed solutions were periodically recorded (Table 1). The AOC concentration was also measured as described elsewhere (Hammes et al., 2007).

For biofilm sampling, PVC coupons were collected from each reactor every 21 days for 168 days. The coupon biofilm samples were resuspended in 10 mL of sterile phosphate buffer solution (pH = 7.0 ± 0.1) and biofilms were scraped using sterilized blades followed by high-speed vortexing for 15 min. Then, the collected biofilm solutions were homogenized by a tissue-homogenizer. The dissolved organic carbon concentration of the homogenized biofilm solutions was measured. Biofilm samples from HS reactor, AOM reactor, and R2A reactor were labeled as “BHS”, “BAOM”, and “BR2A”, respectively. The remaining samples were saved for further analyses.

2.3. EEM measurements, parallel factor analysis (PARAFAC) modeling, and UV absorbance

The collected feed solutions and biofilm samples were diluted using deionized water (DI) and filtered through 0.45 μm hydrophilic polyethersulfone membrane filters (EMD

Millipore, CA, USA) following the protocols for EEM measurement (Ramesh et al., 2007; Li et al., 2013). The EEM spectra were recorded in triplicate for each sample using a spectrofluorophotometer (RF-6000, Shimadzu, Japan). The scanning ranges were 200–500 nm at 5-nm intervals for excitation (Ex) and 220–560 nm at 2-nm intervals for emission (Em). Readings were collected using a scanning rate of 12,000 nm/min with a slit width of 5.0 nm band pass for both Ex and Em. A total of 120 EEM spectra were collected and processed in MATLAB (MathWorks, Natick, MA) using a drEEM 4.0 toolbox (Murphy et al., 2013). Blank corrections, Raman and Rayleigh scattering removal, and inner-filter corrections were performed according to the procedures implemented in drEEM based on the UV absorbance data and the blank DI water peaks (18.2 MΩ cm, Ex at 350 nm). The obtained EEMs were normalized to the water Raman Unit (R.U.) before other analyses. The ranges for Ex and Em were restricted to 250–450 nm and 270–560 nm for PARAFAC modeling to minimize spectral background noise. Preliminary EEM-PARAFAC models with 1–8 components were tested for all samples. Then, a five-component model was validated using split-half analysis (Murphy et al., 2013) and best described the variation of the entire EEM data set (Table S1). For each model component, the obtained maximum fluorescence intensity (F_{max}; unit: R.U.) was used to represent its relative concentration in samples (Murphy et al., 2013; Cai et al., 2017; Watson et al., 2018). The UV absorbance at 203 nm, 253 nm, and 254 nm was also recorded in triplicate using a UV spectrophotometer (UV–Vis, 1800; Shimadzu, Japan) and their ratios (previously reported indicators for DBP formation) were calculated (Kim and Yu, 2007; Yan et al., 2011; Hua et al., 2017).

2.4. DBP formation potential tests and DBP analytical methods

DBP formation potential (DBPFP) tests were conducted based on the standard method 5710B (Rice et al., 2012; Wang et al., 2012b). In order to correlate DBPFP results to the outcomes of EEM and UV absorbance analyses, which require filtration with 0.45 μm membrane for sample preparation, homogenized biofilm samples for DBPFP tests were also filtered using the same membrane filter. A portion of filtered biofilm samples was transferred to 40 mL glass vials, which were filled completely without headspace by adding additional phosphate buffer solution to adjust the final dissolved organic matter concentration to 2 mg/L. Then, samples were treated by excessive amounts of Cl_2 and incubated in darkness for 5 days at room temperature. The chlorine dosage was determined by preliminary chlorine demand tests and more details are described in the Text S1. The residual chlorine was measured using the DPD method and quenched by ~50 mg of NH_4Cl (Rice et al., 2012). Lastly, DBPs were extracted and analyzed by a gas chromatography (Shimadzu, Japan, GC-2010 Plus) using dual electron-capture detectors. For carbonaceous DBPs (C-DBPs), we measured (1) three haloacetic acid (HAA_3) species including monochloroacetic acid (MCAA), dichloroacetic acid (DCAA), and trichloroacetic acid (TCAA), (2) trichloromethane (TCM; the only detected trihalomethanes (THMs)), and (3) two haloketone (HK_2) species including 1,1-dichlro-2-propanone (1,1-DCP) and 1,1,1-trichloropropanone (1,1,1-TCP). For nitrogenous DBPs (N-DBPs), we measured two haloacetonitrile (HAN_2) species including trichloroacetonitirile (TCAN) and dichloroacetonitrile (DCAN), and trichloronitromethane (TCNM). Since no additional bromide was added to the biofilm samples, brominated DBP formation was negligible. HAAs were measured according to EPA Method 552.2, while THMs, HKs, HANs, and

TCNM were measured according to EPA Method 551.1 with small modifications (Reckhow, 2012; Wang et al., 2012b). More analysis details and quality control methods are available elsewhere (Wang et al., 2012b, 2013b). The mass-based DBPFP results were presented as DBP yield (μg/mg-C).

2.5. Statistical analyses

All the statistical analyses were conducted using XLSTAT software (Anddinsoft, Paris, French). Pearson correlation was performed to examine the relationships among the derived EEM-PARAFAC components, selected UV indicators, and DBP formation of biofilms. The results were presented as the coefficient of determination (R^2) and visualized using heatmap. The correlation was statistically significant when $P < 0.05$. Multiple linear regression models were also built to predict the DBP formation of biofilms.

3. Results and discussion

3.1. DBP formation from biofilms

Fig. 1 shows the dynamic changes of DBP yields among biofilm samples. The yields of HAA_3, HK_2, and N-DBPs for BHS had the maximum values at day 42, while the yields of TCM were similar at days 21, 42, and 63 (37.20 ± 2.15 μg/mg-C). For BAOM, the maximum DBP yields for all the examined DBPs were found at day 21, and decreasing trends were observed after this sampling point. However, all DBP yields started to increase from day 147 on. The HAA_3 and HK_2 yields of BR2A had similar patterns that began to decrease from the maximum values at day 42, while they tended to have gradually increasing trends starting from day 105. The minimum yields of TCM (15.98 ± 2.43 μg/mg-C) and N-DBPs (1.28 ± 0.11 μg/mg-C) for BR2A were observed at day 84 and 105, respectively. Overall, BAOM produced much higher levels of both C-DBPs and N-DBPs than BR2A from day 21–105 and BHS throughout the entire study. For the DBP speciation, DCAA formation was higher than TCAA among HAA_3 for all biofilm samples. For HK_2, 1,1,1-TCP was the dominant species, as 1,1,1-DCP can be further oxidized under the presence of excessive amounts of chlorine (Yang et al., 2007). Among the HAN_2, DCAN was the predominant species (85.59 ± 14.41%; Table S2), which was in agreement with the prior studies related to the DBP yields of bacterial EPS (Wang et al., 2012b, 2013b).

Apart from the biofilms' DBP yields, the DBP yields of HS, AOM, and R2A feed solutions were also tested. Significant differences were found between the DBP yields of biofilm samples and their corresponding feed solutions (Fig. 1). For example, among the studied HAA_3, DCAA was the predominant HAA species from BHS (49.55 ± 5.85%), while TCAA (58.12 ± 3.67%) was the major species of the HS feed solution. A previous study indicated that DCAA precursors were mostly hydrophilic, while TCAA precursors were mainly hydrophobic (Hong et al., 2013). Besides being an indicator for aromatic compounds in water, it has been reported that $SUVA_{254}$ is also associated with the hydrophobicity of the organic compounds, where the natural waters with $SUVA_{254} > 2.0$ L/mg-m generally are hydrophobic (Ates et al., 2007; Bekaroglu et al., 2010). In our study, all the biofilm samples which exhibited strong hydrophilic properties with $SUVA_{254} < 0.9$ L/mg-m preferentially produced higher DCAA than TCAA (Fig. 1a). However, compared to biofilms, the HS feed

solution with more hydrophobic characteristics ($SUVA_{254}$ = 2.17 L/mg-m; Table 1) produced higher TCAA than DCAA (Fig. 1a). For N-DBP formation, it is worth noting that previous studies indicated that nitrogen-rich materials such as bacteria had higher N-DBP formation (e.g., 2–3 μg-HAN/mg-C) than HS (e.g., <2 μg-HAN/mg-C) (Wang et al., 2013a, 2015). In contrast, we observed that both HAN and TCNM yields of BHS (<2.03 μg-HAN/mg-C and <1.37 μg-TCNM/mg-C) were lower than those of the corresponding HS feed solutions (3.73 μg-HAN/mg-C and 6.81 μg-TCNM/mg-C). The differences between N-DBP yields of HS in our study and those of the aforementioned previous studies may be due to the effects of ozone treatment, as pre-ozonation prior to chlorination can significantly change the formation of N-DBPs (Chiang et al., 2010; Chu et al., 2012; Xie et al., 2013). An increase of HAN and TCNM formation were previously found after ozone treatment due to the production of abundant low molecular weight organic nitrogen, which is one of the most important precursors for N-DBPs. Consequently, these changes could further impact the differences in HAN and TCNM yields between BHS and HS feed solutions.

3.2. EEM-PARAFAC analysis

Two distinct classes of fluorophores, humic and protein-like fluorophores, are typically found and used to characterize DBP precursors, and the characteristics of these two fluorophores vary from sample to sample (Fellman et al., 2010). In this study, a five-component model with 97.60% of explained variance was obtained and validated using split-half analysis (Fig. 2 & Table S1). Table S3 shows the maxima excitation and emission wavelength of each component, as well as the descriptions of similar components identified from previous studies. Briefly, the characteristics of EEM spectra suggested that Component 1 (C1), Component 2 (C2), and Component 3 (C3) could be classified as protein-like components, while Component 4 (C4) and Component 5 (C5) could be classified as humic-like components. C1 exhibited a single excitation/emission wavelength pair of 275 nm/314 nm (Fig. 2a), similar to tyrosine-like substances (Leenheer and Croué, 2003; Mermillod-Blondin et al., 2015). C2 had two excitation maxima (at 265 nm and 285 nm) and an emission maximum (at 288 nm) in its fluorescence fingerprints (Fig. 2b). It was located at the soluble microbial byproduct-like substance region (Region II) as previously described (Chen et al., 2003). C3 was composed of a primary and secondary fluorescence peak at an excitation/emission wavelength of 255 (280) nm/326 nm (Fig. 2c), belonging to tryptophan-like substances (Coble, 2007). C4 was characterized by fluorescence peaks at 300 nm for excitation and 420 nm for emission (Fig. 2d), representing a low molecular weight humic-like substances (Murphy et al., 2006; Fellman et al., 2010). C5 was a high molecular weight humic-like substances (Murphy et al., 2006; Fellman et al., 2010) with a primary and secondary fluorescence peak at an excitation/emission wavelength of 275 (320) nm/462 nm (Fig. 2e).

3.3. Chemical compositions of biofilms characterized by EEM

Although the chemical compositions of biofilms have been previously studied by the fluorescence EEM technique coupled with either traditional peak picking or fluorescence regional integration method (Matar et al., 2016; Miao et al., 2017; Pérez and Susa, 2017), to our knowledge, this is the first study that applies the EEM-PARAFAC model to characterize biofilm components. Notably, to be compatible with the DBP yield results (Fig. 1), the

results of EEM-PRAFAC were also normalized by the carbon concentration and presented as F_{max} (R.U.)/mg-C (Fig. 3a). In addition, to exhibit the relative abundance of components in each sample, F_{max}% values were calculated (Fig. 3b). We found higher total fluorescence compounds in the HS feed solutions compared to the AOM and R2A feed solutions under the same carbon concentration (Fig. 3a & Table 1). On the other hand, in accordance with the dynamic trends of DBP yield results, strong fluctuations were also observed for the F_{max} (R.U.)/mg-C and F_{max}% values of the identified EEM-PARAFAC components within BHS, BAOM, and BR2A at different sampling points (Fig. 3). From day 21–105, higher F_{max} (R.U.) per unit carbon was observed in BAOM than BHS and BR2A; however, this trend disappeared from day 126 on. In the HS reactor, although the feed solution possessed more than 70% of humic-like components (C4 and C5), protein-like components (C1, C2, and C3) were always the predominant compounds in BHS from day 21 on. Within the AOM reactor, around 45.16% of protein-like components were present in the feed solution, which was much higher than those in the HS reactor (27.14%). At day 21, the highest F_{max} (R.U.)/mg-C was observed in BAOM compared to all other samples. At this sampling point, BAOM also contained a much higher percentage of C4 (16.73%) compared to BHS (3.41%) and BR2A (4.49%). However, this percentage dropped to 1.33% at day 42 and showed a relative abundance of 3.05 ± 1.40% in BAOM in the remaining sampling points. In the R2A reactor, the highest amounts of protein-like substances were consistently present in the R2A feed solution (85.92%) compared to the other two feed solutions and their relative abundance in BR2A varied over time, ranging from 87.55% to 95.34%.

It is well reported that humic-like components are essential for some biological activities [e.g., acting as electron donor or acceptor for microbial respiration (Flemming and Wingender, 2010)], however, the quantitative amounts of these compounds in biofilms are rarely explored. In this study, we observed that the protein-like components (89.73 ± 3.96%) are around nine-fold higher than those of humic-like components (10.27 ± 3.96%) in all the biofilm samples although they were fed with HS, AOM, and R2A solutions, respectively with distinctive chemical compositions. Throughout the study, although the same feed solutions were continuously provided to the corresponding reactors, the F_{max} (R.U.)/mg-C and F_{max}% values of each EEM-PARAFAC component in biofilms showed strong temporal changes across all the samples. Several factors can be responsible for these dynamic changes. First, the microbial community composition in different reactors can be shifted in response to the organic matter characteristics in the feed solutions (Li et al., 2019). Thus, depending on the EPS biosynthesis pathway of the microorganisms in BHS, BAOM, and BR2A, the production of certain biofilm EPS compounds can be promoted or inhibited, leading to the variations of EEM-PARAFAC components within biofilms (Schmid et al., 2015; Li et al., 2019). Second, we observed continuous biofilm development in our previous study (Li et al., 2019), which implied that the available substrate in the feed solution could be utilized by biofilms. Depending on the levels of biological activity, different amounts of organic substrates in feed solutions could be degraded by microbial cells and be transformed into biofilm compounds, partially affecting the chemical compositions of biofilms (Liu and Li, 2010; Wang et al., 2013a). Moreover, biofilm is a complex matrix with various binding sites that could trap a wide range of substances (Flemming, 1995; Wang et al., 2012a). Those adsorbed compounds from feed solution could be accumulated, becoming parts of

biofilm EPS, and/or be degraded via biological processes, thus contributing to the dynamics of the chemical compositions of biofilms.

Collectively, the results of EEM-PARAFAC components and DBP yields suggested that through a series of biological processes (including biotransformation and biosorption of organic matter), the ozonated organic compounds in feed solutions can be continuously metabolized or accumulated in biofilms (Camper, 2004; Wang et al., 2012a), leading to the unique DBP yields varying over time upon chlorine reactions. Currently, for biofilm research, it has been a great challenge to differentiate the produced and adsorbed compounds in biofilm matrices (Wingender et al., 1999). To enhance our understanding on the complex biofilm-derived DBP precursors, further studies are required to investigate the relative contribution of biotransformation and biosorption of the ozonated organic matter that affects the chemical compositions of biofilms and subsequent DBP yields.

3.4. Correlations between EEM-PARAFAC components and the derived-DBPs

Pearson correlation analysis was conducted to determine the correlations between potential predictors and the DBP yields of biofilms (Fig. 4). Since all the correlation coefficients are positive, the results were presented as the coefficient of determination (R^2). Numerous studies have investigated the possibility of applying UV absorbance to estimate DBP formation. For example, it was reported that $SUVA_{254}$, a surrogate for the aromaticity, correlated well with HAA, THM, and the unknown total organic halogen formation (Ates et al., 2007). The ratio of A253/A203, which indicates the substitution tendency of the organic compounds, has also been found to be well correlated with HAA ($R^2 = 0.99$) and THM ($R^2 = 0.99$) formation of different water samples collected from water treatment plants (Kim and Yu, 2007). However, in our study, these two UV indicators were weakly correlated with the DBP yields of biofilms ($R^2 = 0.29–0.50$, $P < 0.05$). These results suggested that $SUVA_{254}$ and A253/A203 cannot effectively capture the reactive sites in biofilms responsible for DBP formation.

On the other hand, the F_{max} values of EEM-PARAFAC components C1, C2, C3, and C5 generally showed much better correlations with all the DBP yields of biofilms ($R^2 = 0.56–0.88$, $P < 0.05$) than $SUVA_{254}$ and A253/A203. C1 (tyrosine-like substances) and C3 (tryptophan-like substances) are aromatic proteins (Chen et al., 2003), but compared to C1, C3 may indicate more intact proteins or less degraded peptide compounds (Fellman et al., 2010). The DBP yields of pure tyrosine and tryptophan have been studied previousely and the studies reported that upon chlorination, tryptophan produced the highest amounts of TCNM as well as HAAs and THMs compared to tyrosine and other amino acids (e.g., asparagine, lysine, serine, glutamic acid, etc.), while the DCAN formation of tyrosine and tryptophan was similar (Hong et al., 2009; Yang et al., 2012). In addition to C1 and C3, another protein-like component, C2 (soluble microbial byproduct-like substances), is a critical DBP precursor (Liu and Li, 2010; Liu et al., 2014; Shen et al., 2016). Soluble microbial byproduct-like substances can be formed during substrate metabolism by microorganisms or from the biomass decay (Barker et al., 2000; Ni et al., 2010). The release of soluble microbial byproduct-like substances from biofilms has been reported to increase the DBP yields (e.g., HAAs, THMs, HANs, and N-nitrosodimethylamine) of filter effluent

in drinking water treatment plants (Shen et al., 2016; Liu et al., 2017). Moreover, a recent study reported that soluble microbial byproduct-, tyrosine-, and tryptophan-like components found in algal intracellular organic matter mainly comprised of carbon- and nitrogen-rich substances with aromatic/aliphatic structures (Hua et al., 2019). These structures can be vital DBP precursors if their chain structures are linked to the electron-donating functional groups such as -S-, $–NH_2$, and –OH (Hong et al., 2009; Hua et al., 2017). We found that all of the studied DBPs had the best correlations with the F_{max} values of tryptophan-like substances (C3) in biofilms than other components ($R^2_{min} \geq 0.76$, $P < 0.05$; Fig. 4), which suggested that C3 had the strongest tendency to form DBPs in biofilm matrices upon chlorine reaction. At given sampling points, the biofilm samples with higher C3 content could result in more DBP yields. For example, the higher C3 content in BAOM than BHS across the entire study, as well as in BAOM than BR2A from day 21–126 was possibly the major cause for the elevated DBP yields of BAOM, compared to BHS or BR2A, in the corresponding periods (Fig. 1, Fig. 3).

Besides protein-like components, the F_{max} values of two humic-like components C4 (low molecular weight humic-like substances) and C5 (high molecular weight humic-like substances) were also correlated to the DBP yields of biofilms ($R^2 = 0.22–0.78$, $P < 0.05$). However, the correlation levels of C4 were poor ($R^2_{max} \leq 0.43$, $P < 0.05$). The humic-like components derived from algal intracellular organic matter contain less nitrogen or more oxygen molecule content, which is associated with carboxyl groups (Hua et al., 2019). These carboxylic groups could be electron-withdrawing functional groups that decrease the reactivity of the adjacent carbons, suppressing the chlorine substitution (Hua et al., 2017). Thus, C4 may be considered as a minor DBP precursor in biofilms as it exhibited the lowest propensity in forming DBPs. However, compared to C4, the other humic-like component, C5 showed better correlations with the studied DBPs ($R^2 = 0.56–0.78$, $P < 0.05$). The differences between C4 and C5 with regards to DBP yields may be explained by their derived-sources. According to previous studies, C4 was commonly found in marine environments associated with biological activities (Stedmon and Markager, 2005; Fellman et al., 2010), while C5 was mostly terrestrial plant or soil organic matter-derived (Fellman et al., 2010). In this study, it can be surmised that C5 may be the intact or less biofilm degraded humic-like substances, while C4 may represent the compound derived from the oxidative cleavage of C5 in the ozonation process during feed solution preparation and the biodegradation of C5 by biofilms.

Based on the correlation level data, multiple linear regression models were further developed to predict the DBP formation of biofilms (Table S4). For the model development, C4, $SUVA_{254}$, and A253/A203 were not included as predictor variables for the DBP yields due to their weak correlations. Notably, the combination of the F_{max} values of the C1, C2, C3, and C5 substantially improve the predictability of the studied DBPs ($R_{min} \geq 0.80$, $P < 0.05$; Table S4) compared to the individual EEM-PARAFAC components ($R_{min} \geq 0.56$, $P < 0.05$; Fig. 4), confirming that each of these components contributed a part of the DBP precursor pool in biofilms. In previous DBP-related works, lab-scale based DBP prediction models were often established as a benchmark to provide quantitative and mechanistic insight for DBP formation, although they might not be applicable to a broad range of samples (Hua et al., 2018; Ma et al., 2018). For future research, further analysis and validation will be needed

to evaluate and improve our obtained models for a wide array of biofilm samples collected from different EWS.

4. Conclusions and engineering implications

Our work investigated the applicability of the EEM-PARAFAC technique for monitoring the chemical compositions of biofilms under ozonated HS and AOM as well as R2A media for 168 days. The results revealed that the chemical compositions of biofilms could be characterized by three protein-like components (C1, C2, and C3) and two humic-like components (C4 and C5). The ozonated organic compounds in the feed solution can be accumulated and transformed, leading to the dynamic changes of EEM-PARAFAC components in biofilms. Along with these changes, the DBP yields of biofilms, which varied over time, were distinctively different from the feed solutions. Overall, BAOM had both higher C-DBP and N-DBP yields than BHS. The Pearson correlation analysis results indicated that compared to UV indicators, EEM-PARAFAC components (C1, C2, C3, and C5) were more effective to capture the reactive sites in biofilms for DBP formation. C3 (tryptophan-like substances) was the best-correlated component to the DBP yields of biofilms, while C4 (low molecular weight humic-like substances) had the lowest tendency to form DBPs. The derived multiple linear regression models from C1, C2, C3, and C5 ($R^2_{min} \geq 0.80$, $P < 0.05$) also provide quantitative insights to estimate the DBP yields of biofilms.

To maintain biological stability in EWS, controlling biofilms by disinfection is critical (Liu et al., 2016). However, the reactions between disinfectants and biofilms inevitably lead to the formation of toxic DBPs. Compared to the planktonic microbial cells, biofilms are more resistant, therefore, they can survive even under constant exposure to disinfectants, continuously serving as reservoirs for DBP precursors (Wang et al., 2013a; Otter et al., 2015; Liu et al., 2016). Our study provides evidence that the DBP formation of biofilms is distinctive, which can play a crucial role in DBP formation and speciation in EWS. Depending on the chemical compositions of biofilms, the subsequently derived DBPs can deteriorate the water quality at varying levels. In addition, since biofilms are heterogeneous, the physical structure of biofilm (e.g., biofilm thickness, surface roughness, porosity, and biomass density) is another intrinsic factor that can significantly impact the disinfectant transport and penetration in biofilms and result in different levels of disinfectant decay and subsequent DBP formation (Xue and Seo, 2013; Xue et al., 2014; Xu et al., 2018). Thus, for future research, designing specific experiments and sampling strategies to elucidate the interplaying roles of the chemical and physical characteristics of biofilm on biofilm-derived DBP formation is necessary to further unravel the deeper mechanisms of DBP formation from biofilms. Practically, to optimize the EWS operation and disinfection practices, preliminary assessments and surveys for the chemical and physical structures of biofilms are recommended to evaluate both disinfection efficacy and the potential risks associated with the biofilm-derived toxic DBP formation. To date, many water utilities begin to adopt various biofilm monitoring devices (e.g., *in situ* coupons) to maintain the biological stability of EWS. Our results suggested that along with current efforts to monitor and control biofilms, EEM-PARAFAC technique is a simple and promising monitoring tool that can provide valuable qualitative and quantitative insights to improve the disinfection protocol and predict the biofilm-derived DBP formation in EWS.

Supplementary Material

Refer to Web version on PubMed Central for supplementary material.

Acknowledgements

This study was supported by the National Science Foundation of United States (CBET 1236433 & 1605185), the Ohio Water Development Authority (7174), the Ohio Department of Higher Education (R/SDW-2-BOR) and in part by the U.S. Environmental Protection Agency. Any opinions expressed do not reflect the views of the agency; therefore, no official endorsement should be inferred. Any mention of trade names or commercial products does not constitute endorsement or recommendation for use. Authors also appreciate Ms. Faith Seo and Emily Briese for proofreading the early version of the manuscript, and Anusha Kadudula for assisting the AOC analysis.

References

Abokifa et al, 2016. Abokifa AA, Yang YJ, Lo CS, Biswas P. Investigating the role of biofilms in trihalomethane formation in water distribution systems with a multicomponent model Water Res, 104 (2016), pp. 208–219 [PubMed: 27525584]

Ates et al, 2007. Ates N, Kitis M, Yetis U. Formation of chlorination by-products in waters with low SUVA—correlations with SUVA and differential UV spectroscopy Water Res, 41 (2007), pp. 4139–4148 [PubMed: 17614116]

Baribeau, 2006. Baribeau H.l. Formation and Decay of Disinfection By-Products in the Distribution System American Water Works Association (2006)

Barker et al, 2000. Barker DJ, Salvi SM, Langenhoff AA, Stuckey DC Soluble microbial products in ABR treating low-strength wastewater J. Environ. Eng, 126 (2000), pp. 239–249

Batmanghelich et al, 2017. Batmanghelich F, Li L, Seo Y. Influence of multispecies biofilms of Pseudomonas aeruginosa and Desulfovibrio vulgaris on the corrosion of cast iron Corros. Sci, 121 (2017), pp. 94–104

Bekaroglu et al, 2010. Bekaroglu SK, Yigit N, Karanfil T, Kitis M. The adsorptive removal of disinfection by-product precursors in a high-SUVA water using iron oxide-coated pumice and volcanic slag particles J. Hazard Mater, 183 (2010), pp. 389–394

Cai et al, 2017. Cai W, Liu J, Zhu X, Zhang X, Liu Y. Fate of dissolved organic matter and byproducts generated from on-line chemical cleaning with sodium hypochlorite in MBR Chem. Eng. J, 323 (2017), pp. 233–242

Camper, 2004. Camper AK Involvement of humic substances in regrowth Int. J. Food Microbiol, 92 (2004), pp. 355–364 [PubMed: 15145594]

Chen et al, 2003. Chen W, Westerhoff P, Leenheer JA, Booksh K. Fluorescence excitation− emission matrix regional integration to quantify spectra for dissolved organic matter Environ. Sci. Technol, 37 (2003), pp. 5701–5710 [PubMed: 14717183]

Chiang et al, 2010. Chiang P-C, Chang E-E, Chuang C-C, Liang C-H, Huang C-P Evaluating and elucidating the formation of nitrogen-contained disinfection by-products during pre-ozonation and chlorination Chemosphere, 80 (2010), pp. 327–333 [PubMed: 20427073]

Chu et al, 2012. Chu W, Gao N, Yin D, Deng Y, Templeton MR Ozone–biological activated carbon integrated treatment for removal of precursors of halogenated nitrogenous disinfection by-products Chemosphere, 86 (2012), pp. 1087–1091 [PubMed: 22205050]

Coble, 1996. Coble PG Characterization of marine and terrestrial DOM in seawater using excitation-emission matrix spectroscopy Mar. Chem, 51 (1996), pp. 325–346

Coble, 2007. Coble PG Marine optical biogeochemistry: the chemistry of ocean color Chem. Rev, 107 (2007), pp. 402–418 [PubMed: 17256912]

Coburn et al, 2016. Coburn KM, Wang Q, Rediske D, Viola RE, Hanson BL, Xue Z, Seo Y. Effects of extracellular polymeric substance composition on bacteria disinfection by monochloramine: application of MALDI-TOF/TOF–MS and multivariate analysis Environ. Sci. Technol, 50 (2016), pp. 9197–9205 [PubMed: 27366970]

Di Tommaso et al, 2019. Di Tommaso C, Taylor-Edmonds L, Andrews SA, Andrews RC The contribution of biofilm to nitrogenous disinfection by-product formation in full-scale cyclically-operated drinking water biofilters Water Res, 155 (2019), pp. 403–409 [PubMed: 30856522]

Fellman et al, 2010. Fellman JB, Hood E, Spencer RG Fluorescence spectroscopy opens new windows into dissolved organic matter dynamics in freshwater ecosystems: a review Limnol. Oceanogr, 55 (2010), pp. 2452–2462

Flemming, 1995. Flemming H-C Sorption sites in biofilms Water Sci. Technol, 32 (1995), p. 27

Flemming and Wingender, 2010. Flemming H-C, Wingender J. The biofilm matrix Nat. Rev. Microbiol, 8 (2010), p. 623 [PubMed: 20676145]

Griffini et al, 1999. Griffini O, Bao M, Barbieri K, Burrini D, Santianni D, Pantani F Formation and Removal of Biodegradable Ozonation By-Products during Ozonation-Biofiltration Treatment: Pilot-Scale Evaluation (1999)

Hammes et al, 2007. Hammes F, Meylan S, Salhi E, Köster O, Egli T, Von Gunten U. Formation of assimilable organic carbon (AOC) and specific natural organic matter (NOM) fractions during ozonation of phytoplankton Water Res, 41 (2007), pp. 1447–1454 [PubMed: 17321564]

Henderson et al, 2009. Henderson RK, Baker A, Murphy K, Hambly A, Stuetz R, Khan S. Fluorescence as a potential monitoring tool for recycled water systems: a review Water Res, 43 (2009), pp. 863–881 [PubMed: 19081598]

Hong et al, 2013. Hong H, Huang F, Wang F, Ding L, Lin H, Liang Y. Properties of sediment NOM collected from a drinking water reservoir in South China, and its association with THMs and HAAs formation J. Hydrol, 476 (2013), pp. 274–279

Hong et al, 2009. Hong H, Wong M, Liang Y. Amino acids as precursors of trihalomethane and haloacetic acid formation during chlorination Arch. Environ. Contam. Toxicol, 56 (2009), pp. 638–645 [PubMed: 18712495]

Hua et al, 2019. Hua L-C, Chao S-J, Huang C. Fluorescent and molecular weight dependence of THM and HAA formation from intracellular algogenic organic matter (IOM) Water Res, 148 (2019), pp. 231–238 [PubMed: 30388524]

Hua et al, 2018. Hua L-C, Lin J-L, Chao S-J, Huang C. Probing algogenic organic matter (AOM) by size-exclusion chromatography to predict AOM-derived disinfection by-product formation Sci. Total Environ, 645 (2018), pp. 71–78 [PubMed: 30015120]

Hua et al, 2017. Hua L-C, Lin J-L, Chen P-C, Huang C. Chemical structures of extra-and intra-cellular algogenic organic matters as precursors to the formation of carbonaceous disinfection byproducts Chem. Eng. J, 328 (2017), pp. 1022–1030

Huang et al, 2013. Huang H, Wu Q-Y, Tang X, Jiang R, Hu H-Y Formation of haloacetonitriles and haloacetamides during chlorination of pure culture bacteria Chemosphere, 92 (2013), pp. 375–381 [PubMed: 23402924]

Kim and Yu, 2007. Kim H-C, Yu M-J Characterization of aquatic humic substances to DBPs formation in advanced treatment processes for conventionally treated water J. Hazard Mater, 143 (2007), pp. 486–493 [PubMed: 17092645]

Leenheer and Croué, 2003. Leenheer JA, Croué J-P Peer Reviewed: Characterizing Aquatic Dissolved Organic Matter ACS Publications (2003)

Li et al, 2019. Li L, Jeon Y, Lee S-H, Ryu H, Santo Domingo JW, Seo Y. Dynamics of the physiochemical and community structures of biofilms under the influence of algal organic matter and humic substances Water Res, 158 (2019), pp. 136–145 [PubMed: 31026675]

Li et al, 2013. Li W-T, Xu Z-X, Li A-M, Wu W, Zhou Q, Wang J-N HPLC/HPSEC-FLD with multi-excitation/emission scan for EEM interpretation and dissolved organic matter analysis Water Res, 47 (2013), pp. 1246–1256 [PubMed: 23260178]

Liu et al, 2017. Liu C, Olivares CI, Pinto AJ, Lauderdale CV, Brown J, Selbes M, Karanfil T. The control of disinfection byproducts and their precursors in biologically active filtration processes Water Res, 124 (2017), pp. 630–653 [PubMed: 28822343]

Liu and Li, 2010. Liu J.-l., Li X.-y. Biodegradation and biotransformation of wastewater organics as precursors of disinfection byproducts in water Chemosphere, 81 (2010), pp. 1075–1083 [PubMed: 20943251]

Liu et al, 2014. Liu J.-l., Li X.-y., Xie Y.-f., Tang H. Characterization of soluble microbial products as precursors of disinfection byproducts in drinking water supply Sci. Total Environ, 472 (2014), pp. 818–824 [PubMed: 24342087]

Liu et al, 2016. Liu S, Gunawan C, Barraud N, Rice SA, Harry EJ, Amal R. Understanding, monitoring, and controlling biofilm growth in drinking water distribution systems Environ. Sci. Technol, 50 (2016), pp. 8954–8976 [PubMed: 27479445]

Lyon et al, 2014. Lyon BA, Cory RM, Weinberg HS Changes in dissolved organic matter fluorescence and disinfection byproduct formation from UV and subsequent chlorination/chloramination J. Hazard Mater, 264 (2014), pp. 411–419 [PubMed: 24316813]

Ma et al, 2018. Ma C, Xu H, Zhang L, Pei H, Jin Y. Use of fluorescence excitation–emission matrices coupled with parallel factor analysis to monitor C-and N-DBPs formation in drinking water recovered from cyanobacteria-laden sludge dewatering Sci. Total Environ, 640 (2018), pp. 609–618 [PubMed: 29870937]

Matar et al, 2016. Matar G, Gonzalez-Gil G, Maab H, Nunes S, Le-Clech P, Vrouwenvelder J, Saikaly PE Temporal changes in extracellular polymeric substances on hydrophobic and hydrophilic membrane surfaces in a submerged membrane bioreactor Water Res, 95 (2016), pp. 27–38 [PubMed: 26981765]

Mermillod-Blondin et al, 2015. Mermillod-Blondin F, Simon L, Maazouzi C, Foulquier A, Delolme CP Dynamics of dissolved organic carbon (DOC) through stormwater basins designed for groundwater recharge in urban area: assessment of retention efficiency Water Res, 81 (2015), pp. 27–37 [PubMed: 26024961]

Miao et al, 2017. Miao L, Wang C, Hou J, Wang P, Ao Y, Li Y, Yao Y, Lv B, Yang Y, You G. Response of wastewater biofilm to CuO nanoparticle exposure in terms of extracellular polymeric substances and microbial community structure Sci. Total Environ, 579 (2017), pp. 588–597 [PubMed: 27871756]

Murphy et al, 2006. Murphy KR, Ruiz GM, Dunsmuir WT, Waite TD Optimized parameters for fluorescence-based verification of ballast water exchange by ships Environ. Sci. Technol, 40 (2006), pp. 2357–2362 [PubMed: 16646474]

Murphy et al, 2013. Murphy KR, Stedmon CA, Graeber D, Bro R. Fluorescence spectroscopy and multi-way techniques PARAFAC. Analytical Methods, 5 (2013), pp. 6557–6566

Ni et al, 2010. Ni B-J, Zeng RJ, Fang F, Xie W-M, Sheng G-P, Yu H-Q Fractionating soluble microbial products in the activated sludge process Water Res, 44 (2010), pp. 2292–2302 [PubMed: 20060562]

Otter et al, 2015. Otter J, Vickery K, Walker J.d., Pulcini E.d., Stoodley P, Goldenberg S, Salkeld J, Chewins J, Yezli S, Edgeworth J. Surface-attached cells, biofilms and biocide susceptibility: implications for hospital cleaning and disinfection J. Hosp. Infect, 89 (2015), pp. 16–27 [PubMed: 25447198]

Pérez and Susa, 2017. Pérez ML, Susa MR Exopolymeric substances from drinking water biofilms: dynamics of production and relation with disinfection by products Water Res, 116 (2017), pp. 304–315 [PubMed: 28355587]

Pivokonsky et al, 2015. Pivokonsky M, Naceradska J, Brabenec T, Novotna K, Baresova M, Janda V. The impact of interactions between algal organic matter and humic substances on coagulation Water Res, 84 (2015), pp. 278–285 [PubMed: 26255125]

Pivokonsky et al, 2016. Pivokonsky M, Naceradska J, Kopecka I, Baresova M, Jefferson B, Li X, Henderson R. The impact of algogenic organic matter on water treatment plant operation and water quality: a review Crit. Rev. Environ. Sci. Technol, 46 (2016), pp. 291–335

Polanska et al, 2005. Polanska M, Huysman K, Van Keer C. Investigation of assimilable organic carbon (AOC) in flemish drinking water Water Res, 39 (2005), pp. 2259–2266 [PubMed: 15925396]

Ramesh et al, 2007. Ramesh A, Lee D, Lai J. Membrane biofouling by extracellular polymeric substances or soluble microbial products from membrane bioreactor sludge Appl. Microbiol. Biotechnol, 74 (2007), pp. 699–707 [PubMed: 17115206]

Reasoner and Geldreich, 1985. Reasoner DJ, Geldreich E. A new medium for the enumeration and subculture of bacteria from potable water Appl. Environ. Microbiol, 49 (1985), pp. 1–7 [PubMed: 3883894]

Reckhow, 2012. Reckhow DA Analysis of trihalomethanes and related pentane-extractable organic halides Reckhow DA (Ed.) (2012) http://www.ecs.umass.edu/eve/research/sop/THM.pdfhttp://www.ecs.umass.edu/eve/research/sop/THM.pdf

Revetta et al, 2016. Revetta R, Gomez-Alvarez V, Gerke T, Domingo J. Santo, Ashbolt N. Changes in bacterial composition of biofilm in a metropolitan drinking water distribution system J. Appl. Microbiol, 121 (2016), pp. 294–305

Rice et al, 2012. Rice EW, Baird RB, Eaton AD, Clesceri LS Standard Methods for the Examination of Water and Wastewater American Public Health Association, Washington, DC (2012)

Schmid et al, 2015. Schmid J, Sieber V, Rehm B. Bacterial exopolysaccharides: biosynthesis pathways and engineering strategies Front. Microbiol, 6 (2015), p. 496 [PubMed: 26074894]

Shen et al, 2016. Shen H, Chen X, Zhang D, Chen H.-b. Generation of soluble microbial products by bio-activated carbon filter during drinking water advanced treatment and its influence on spectral characteristics Sci. Total Environ, 569 (2016), pp. 1289–1298 [PubMed: 27436775]

Stedmon and Markager, 2005. Stedmon CA, Markager S. Resolving the variability in dissolved organic matter fluorescence in a temperate estuary and its catchment using PARAFAC analysis Limnol. Oceanogr, 50 (2005), pp. 686–697

Terry and Summers, 2018. Terry LG, R.S. Summers Biodegradable organic matter and rapid-rate biofilter performance: a review Water Res, 128 (2018), pp. 234–245 [PubMed: 29107908]

Wang et al, 2015. Wang J-J, Dahlgren RA, Erşan MS, Karanfil T, Chow AT Wildfire altering terrestrial precursors of disinfection byproducts in forest detritus Environ. Sci. Technol, 49 (2015), pp. 5921–5929 [PubMed: 25894116]

Wang et al, 2013a. Wang J-J, Liu X, Ng TW, Xiao J-W, Chow AT, Wong PK Disinfection byproduct formation from chlorination of pure bacterial cells and pipeline biofilms Water Res, 47 (2013), pp. 2701–2709 [PubMed: 23499193]

Wang et al, 2013b. Wang Z, Choi O, Seo Y. Relative contribution of biomolecules in bacterial extracellular polymeric substances to disinfection byproduct formation Environ. Sci. Technol, 47 (2013), pp. 9764–9773 [PubMed: 23866010]

Wang et al, 2012a. Wang Z, Hessler CM, Xue Z, Seo Y. The role of extracellular polymeric substances on the sorption of natural organic matter Water Res, 46 (2012), pp. 1052–1060 [PubMed: 22209278]

Wang et al, 2012b. Wang Z, Kim J, Seo Y. Influence of bacterial extracellular polymeric substances on the formation of carbonaceous and nitrogenous disinfection byproducts Environ. Sci. Technol, 46 (2012), pp. 11361–11369 [PubMed: 22958143]

Watson et al, 2018. Watson K, Farré MJ, Leusch FD, Knight N. Using fluorescence-parallel factor analysis for assessing disinfection by-product formation and natural organic matter removal efficiency in secondary treated synthetic drinking waters Sci. Total Environ, 640 (2018), pp. 31–40 [PubMed: 29852445]

Wingender et al, 1999. Wingender J, Neu TR, Flemming H. Microbial extracellular polymeric substances: characterization, structure and function Structure and Function, 279 (1999)

Xie et al, 2013. Xie P, Ma J, Fang J, Guan Y, Yue S, Li X, Chen L. Comparison of permanganate preoxidation and preozonation on algae containing water: cell integrity, characteristics, and chlorinated disinfection byproduct formation Environ. Sci. Technol, 47 (2013), pp. 14051–14061 [PubMed: 24237350]

Xu et al, 2018. Xu J, Huang C, Shi X, Dong S, Yuan B, Nguyen TH Role of drinking water biofilms on residual chlorine decay and trihalomethane formation: an experimental and modeling study Sci. Total Environ, 642 (2018), pp. 516–525 [PubMed: 29908510]

Xue et al, 2014. Xue Z, Lee WH, Coburn KM, Seo Y. Selective reactivity of monochloramine with extracellular matrix components affects the disinfection of biofilm and detached clusters Environ. Sci. Technol, 48 (2014), pp. 3832–3839 [PubMed: 24575887]

Xue and Seo, 2013. Xue Z, Seo Y. Impact of chlorine disinfection on redistribution of cell clusters from biofilms Environ. Sci. Technol, 47 (2013), pp. 1365–1372 [PubMed: 23256749]

Yan et al, 2011. Yan M, Korshin G, Wang D Characterize Natural Organic Matter in Typical China's Water Using HPLC-SEC with Continuous Wavelength UV Absorbance Detector Speciality Conference on Natural Organic Matter, Costa Mesa, CA (2011), pp. 27–29

Yang et al, 2007. Yang X, Shang C, Westerhoff P. Factors affecting formation of haloacetonitriles, haloketones, chloropicrin and cyanogen halides during chloramination Water Res, 41 (2007), pp. 1193–1200 [PubMed: 17270234]

Yang et al, 2012. Yang X, Shen Q, Guo W, Peng J, Liang Y. Precursors and nitrogen origins of trichloronitromethane and dichloroacetonitrile during chlorination/chloramination Chemosphere, 88 (2012), pp. 25–32 [PubMed: 22425029]

Zhang et al, 2010. Zhang L-S, Wong K-H, Yip H-Y, Hu C, Yu JC, Chan C-Y, Wong P-K Effective photocatalytic disinfection of E. coli K-12 using AgBr− Ag− Bi2WO6 nanojunction system irradiated by visible light: the role of diffusing hydroxyl radicals Environ. Sci. Technol, 44 (2010), pp. 1392–1398 [PubMed: 20085257]

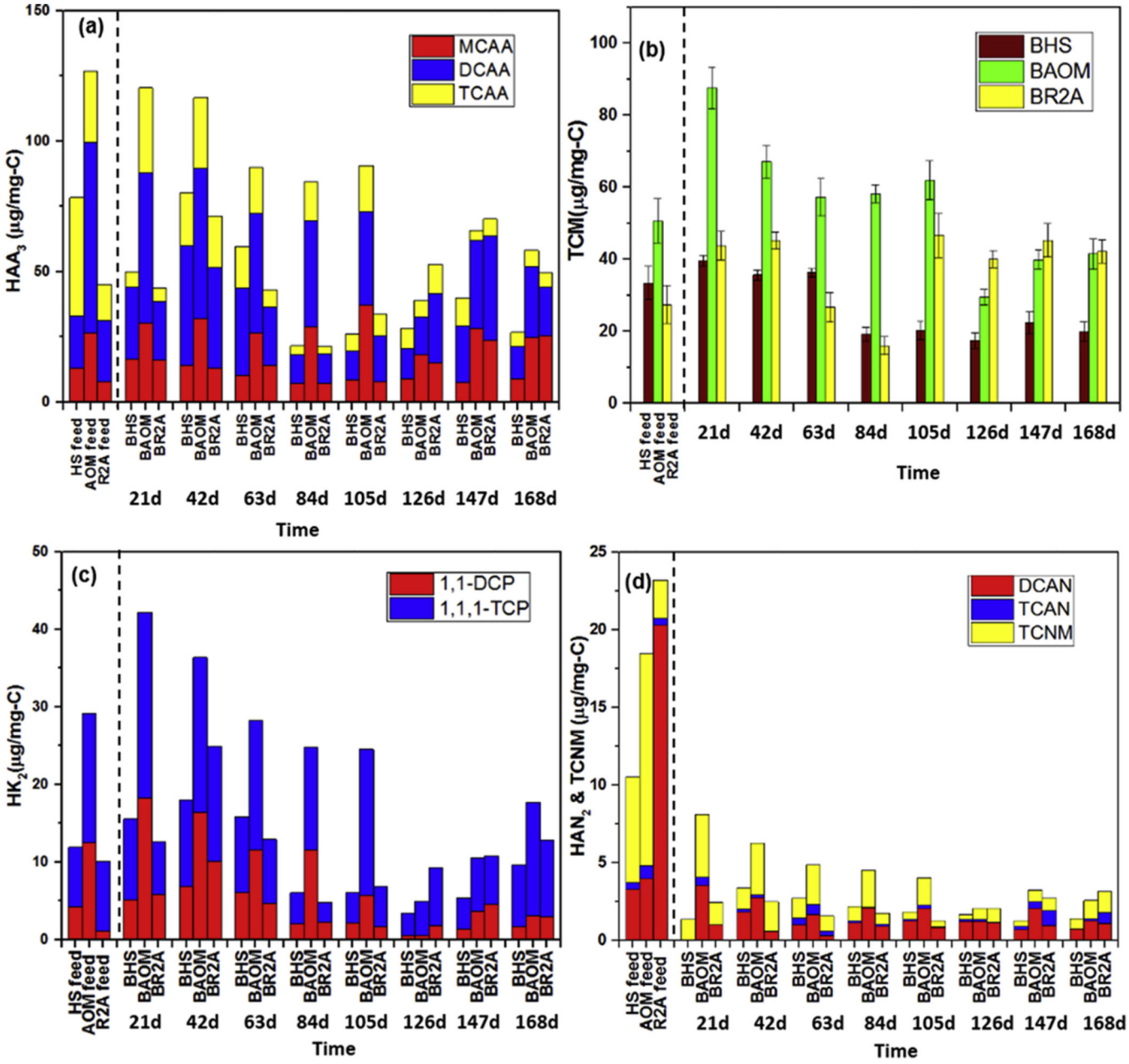

Fig. 1.

Dynamics of (a–c) C-DBP formation and (d) N-DBP formation for biofilms grown under different feed solutions.

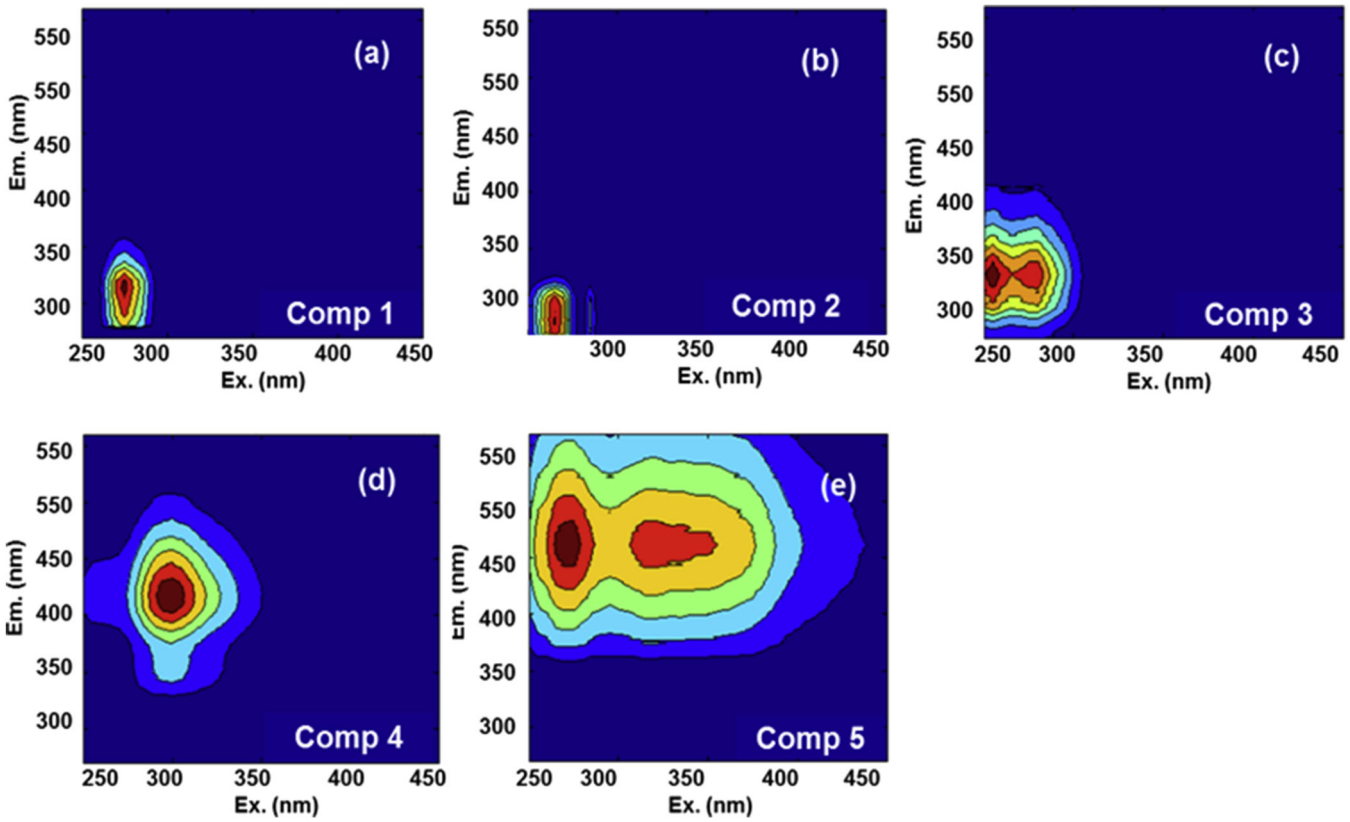

Fig. 2.

Fluorescence fingerprints of the identified EEM-PARAFAC components within biofilms (a–e).

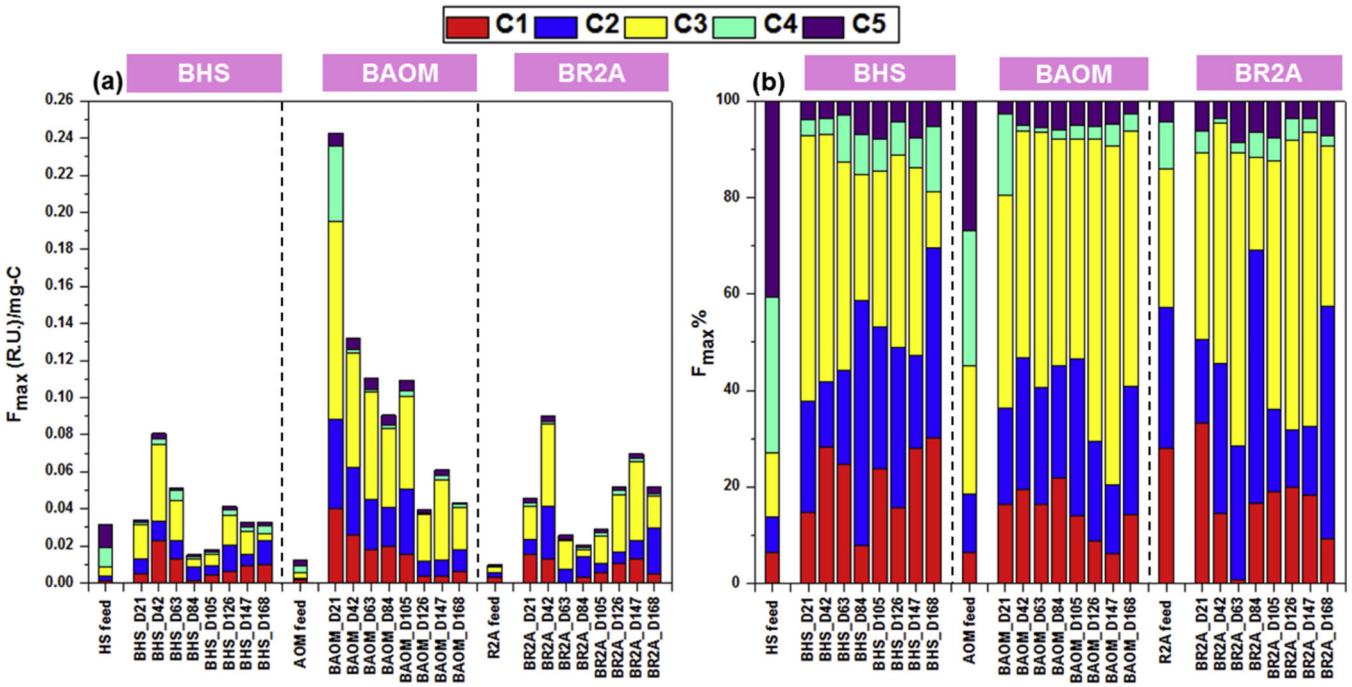

Fig. 3.

The five EEM-PARAFAC components within biofilms and the corresponding feed solutions (a) F_{max} (R.U.)/mg-C and (b) F_{max}%.

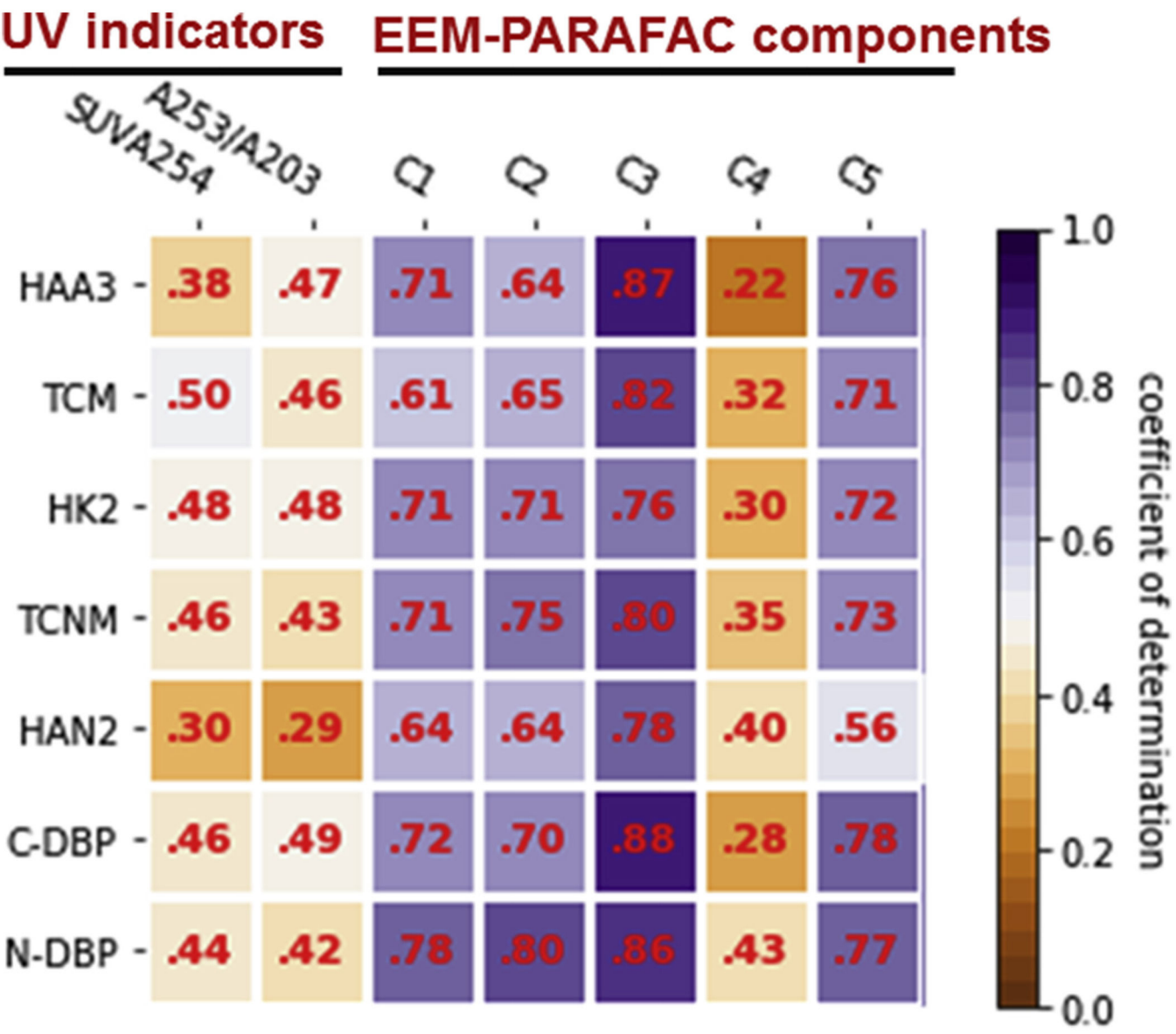

Fig. 4.

Coefficients of determination (R^2) between UV indicators and DBP yields of biofilm, and between F_{max} values of EEM-PARAFAC components and DBP yields of biofilm (n = 24). All the coefficients are statistically significant ($P < 0.05$).

Table 1

Water chemistry of bulk water (reactor influent).

	HS reactor Average ± SD[a]	AOM reactor Average ± SD	R2A reactor Average ± SD
pH	7.80 ± 0.08	7.82 ± 0.04	7.38 ± 0.03
Turbidity (NTU)	1.54 ± 0.23	0.83 ± 0.21	0.15 ± 0.02
PO_4^{3-}(mg/L)	1.14 ± 0.13	1.21 ± 0.25	1.09 ± 0.08
AOC (μg/L)	137.27 ± 9.29	139.27 ± 12.25	140.37 ± 16.23
TOC (mg/L)	1.50 ± 0.21	1.50 ± 0.18	1.50 ± 0.21
$SUVA_{254}$ (L/mg C-m)	2.17 ± 0.31	1.09 ± 0.34	0.57 ± 0.04
TN (mg/L)	1.42 ± 0.37	2.08 ± 0.11	2.51 ± 0.22

[a]represents standard deviation